ORIGINAL ARTICLE

lajss.org
Latin American Journal of Solids and Structures

www.lajss.org

Weak-phase-dominated fracture characteristics and dynamic degradation modeling of coal gangue concrete under cyclic impact

Lei Fan[a,b*], **Yang Liu**[a], **Yanqi Zhu**[a]

[a] School of Mining Engineering, Anhui University of Science and Technology, Huainan, 232001, China. Email: fanlei@aust.edu.cn, 1617407618@qq.com, 2592585189@qq.com
[b] Engineering Laboratory for Safe and Precise Coal Mining of Anhui Province, Anhui University of Science and Technology, Huainan, 232001, China. Email: fanlei@aust.edu.cn

* Corresponding author

https://doi.org/10.1590/10.1590/1679-7825/e8984

Abstract

To support the safe and efficient utilization of coal gangue (CG) as aggregate in underground support structures, this study systematically investigates the dynamic fracture response and damage evolution of coal gangue concrete (CGC) under single and cyclic impact loading. Experimental results show that increasing the CG replacement ratio reduces dynamic strength and elastic modulus while raising peak strain. Under cyclic impact, the impact resistance life shortens significantly, and damage evolution follows a "weak-phase-dominated" mechanism driven by the low strength of CG aggregates and weak interfacial zones. As the replacement ratio increases, failure transitions toward a crushing-dominated mode governed by aggregate fracture and interfacial slip. Based on these findings, a dynamic strength degradation model coupling the replacement ratio and impact number is established to predict residual load-bearing capacity after cyclic impact. This work provides a theoretical basis for the design and safety assessment of CG concrete structures in dynamically disturbed underground environments.

Keywords

coal gangue concrete; dynamic fracture; cyclic impact; damage evolution; degradation model; underground engineering

Graphical Abstract

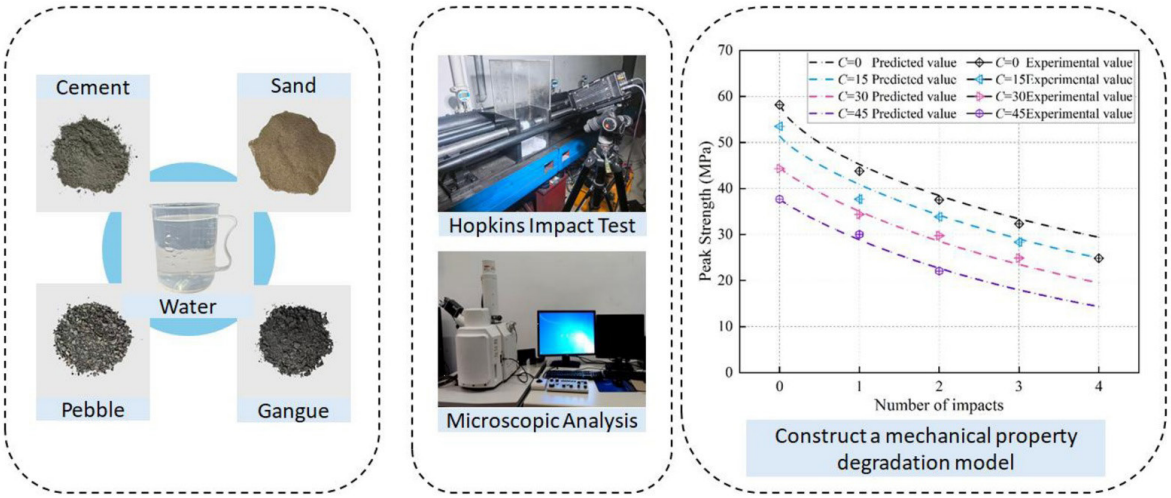

Received January 19, 2026. In revised form January 30, 2026. Accepted February 04, 2026. Available online February 06, 2026.
https://doi.org/10.1590/1679-7825/e8984

1 INTRODUCTION

Coal serves as the primary energy source in China, and its mining process generates massive amounts of coal gangue (CG) solid waste. Currently, China's annual coal production exceeds 4.7 billion tons, with accumulated coal gangue accounting for approximately 10% of coal output and increasing at a rate of about 400 million tons per year, making it one of the largest industrial solid wastes in China (Du et al., 2025). The massive stockpiling of CG not only occupies land resources but also leads to severe environmental pollution and safety risks (Liu & Wang, 2025; Li & Wang, 2019). Against the backdrop of continuous large-scale consumption of natural resources for infrastructure construction, promoting the large-scale resource utilization of CG aligns with the national "dual carbon" strategic goals and represents a vital pathway for achieving coordinated development of mining and the environment (Zhang et al., 2025). Crushing CG for use as coarse aggregate in concrete, especially in applications such as underground roadway support and shotcrete, is widely regarded as a promising consumption pathway (Wu et al., 2025).

To enhance the practical performance of coal gangue concrete (CGC), researchers have incorporated it into concrete as coarse aggregate, fine aggregate, or supplementary cementitious materials (Qin et al., 2025). Studies indicate that the physical and chemical properties of CG aggregate are significantly influenced by its carbon content: lower loss on ignition and carbon content generally correspond to lower crushing value, water absorption, and better soundness. However, uniformly distributed carbon as a defect phase can easily trigger "secondary side effects" and "window opening effects," adversely affecting concrete durability (Jiao et al., 2023). To improve its performance, various modification methods have been extensively explored: incorporating mineral admixtures such as fly ash (Ni et al., 2019) and coal gasification slag (Song et al., 2025) helps optimize workability, mechanical properties, and microstructural refinement; adding nano SiO2, polypropylene fibers (Xiang et al., 2024), or basalt fibers (Yang et al., 2021) can effectively enhance mechanical properties and inhibit microcrack propagation. Recent studies have further demonstrated that composite physical-chemical modification techniques can significantly improve the mechanical properties and fracture toughness of CG concrete by strengthening the interfacial transition zone (ITZ) (Zhang et al., 2026). Furthermore, pretreatment methods such as thermal activation and mechanical grinding can stimulate the pozzolanic activity of CG, increasing its reactivity in cement based materials (Chin et al., 2024). In terms of structural applications, CGC has been successfully used in high ductility rapid repair materials (Wang et al., 2022), concrete filled steel tubes (Wang et al., 2024), and CFRP confined components (Zhou et al., 2022). Research confirms that with proper mix design, CGC can meet specific mechanical requirements, although its overall performance generally declines with increasing replacement rates.

However, the safety of CGC faces severe challenges when used in underground roadway support structures. Under mining induced influences, the surrounding rock of roadways undergoes complex stress redistribution and dynamic disturbances, subjecting support structures to dynamic loads such as rockbursts and mining induced tremors (Chen et al., 2025; He & Wang, 2023; Cai et al., 2021). Understanding the fatigue damage and crack evolution in rock-like materials under cyclic loading is crucial for assessing the long-term stability of such environments (Deng et al., 2026). Existing research has predominantly focused on the static mechanical properties of CGC. Extensive testing indicates that replacing natural aggregate with CG aggregate—due to its relatively low intrinsic strength, high porosity, and weak interfacial bonding with cement paste—typically leads to varying degrees of reduction in compressive strength, tensile strength, and elastic modulus of concrete (Zhang et al., 2026). The fracture behavior and crack propagation in materials with inherent flaws or weak interfaces, as monitored by techniques like AE and DIC, are key to understanding such performance degradation (Zhao et al., 2026). This performance degradation trend introduces potential risks for its application in load bearing structures, particularly in dynamically disturbed roadway environments. Currently, research on the dynamic mechanical properties of CGC remains unsystematic. Existing dynamic tests are mostly limited to single impact responses at a single strain rate, failing to adequately reflect the actual stress state in underground environments characterized by multiple impacts and repeated loading unloading cycles. More critically, there is still a lack of systematic multi scale observation and theoretical explanation regarding the damage evolution mechanisms, fragmentation morphology characteristics, and the intrinsic relationship between macroscopic mechanical behavior and mesoscopic failure mechanisms of CGC under impact loading (Hu et al., 2026).

To address these gaps, this study investigates CGC with different CG replacement ratios through a novel combined impact test scheme. The objectives are to: (1) elucidate the evolution of dynamic mechanical properties under single and cyclic impacts; (2) reveal the underlying "weak-phase-dominated" damage mechanism; and (3) establish a coupled degradation model for residual load-bearing capacity. This work provides a theoretical basis for the safety assessment and design of CGC structures in dynamic disturbance environments.

2 DESIGN AND PREPARATION PROCESS

2.1 Material and preparation of concrete specimens

Referencing the actual construction conditions of concrete in coal mine roadways, an experimental scheme was formulated. Impact compression tests were conducted on concrete specimens with CG contents of 0%, 15%, 30%, and 45%. The specimens had a diameter of 50 mm and a height-to-diameter ratio of 1, and were prepared according to standard procedures. The production process included: mixing the slurry, compaction, surface leveling, curing, demolding, secondary surface leveling, and final curing. The secondary leveling process involved using cement mortar to smooth the ends, controlling the unevenness of the concrete specimens. The experimental workflow for the CGC is illustrated in Fig.1.

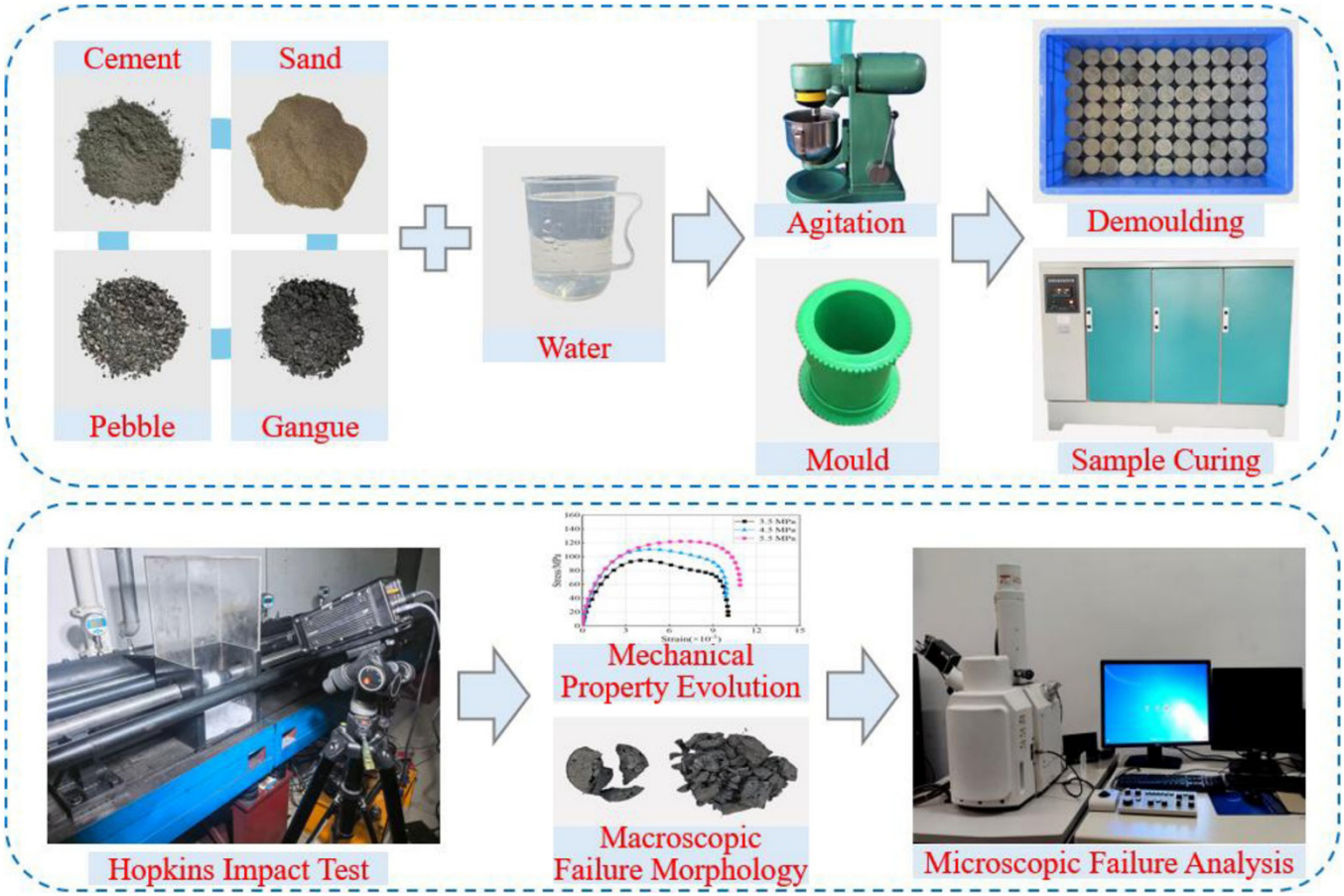

Figure 1. Experimental procedure

The test used Grade 42.5 ordinary Portland cement. The coarse aggregate consisted of metamorphic sandstone, and the fine aggregate was ordinary river sand. To ensure the test specimens accurately reflect the mechanical properties of the concrete, the maximum aggregate diameter was kept smaller than one-fifth of the mold diameter. The concrete mix design is shown in Table 1, and the physical and mechanical indices of the CG are presented in Table 2.

Table 1. Concrete mix ratio

Parameter	Cement (g)	Sand (g)	Gravel (g)	Fly Ash (g)	CG(g)	Water (g)
Value	430	190	800	10	-	200

Table 2. Physical and mechanical indices of CG

Attribute	Particle Size (mm)	Loose Bulk Density (kg/m^3)	Water Absorption Rate (%)	Crushing Value (%)	Compressive Strength (MPa)
Value	3~10	1220	5	12	43

2.2 Test equipment and scheme

Dynamic compression tests were conducted using the SHPB (Split Hopkinson Pressure Bar) test system, as illustrated in Fig. 2. The SHPB setup employs a cylindrical striker with a length of 300 mm. Both the incident bar and transmitted bar have a diameter of 50 mm and are made of 40Cr alloy steel, with a density of 7800 kg/m^3 and a longitudinal wave velocity of 5190 m/s. Prior to testing, the incident and transmitted bars were carefully aligned horizontally and coaxially to ensure minimal generation of reflected waves.

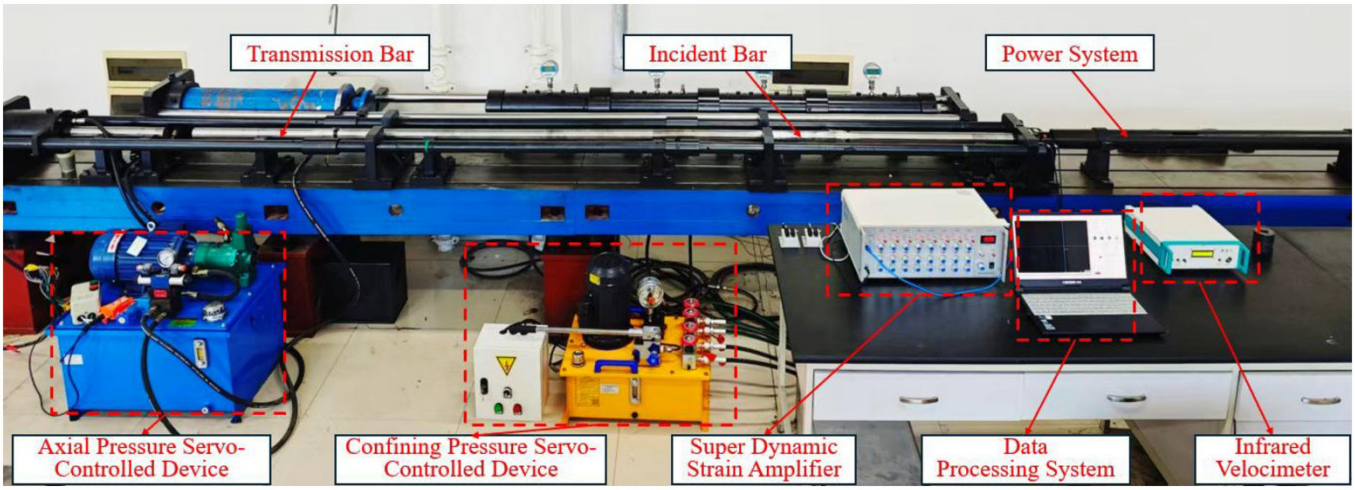

Figure 2. Split Hopkinson Pressure Bar (SHPB) impact testing system

To systematically simulate the combined working conditions of potential accidental high-energy dynamic loads and frequent low-energy disturbances (e.g., mining tremors) that underground roadway support structures may encounter, this study designed a systematic impact scheme as shown in Table 3. The aim is to systematically investigate the influence of CG content on the dynamic mechanical properties of concrete under single and cyclic impact loads. Test specimens were prepared with four replacement ratios (0%, 15%, 30%, and 45%) of CG by volume substituting coarse aggregate. Impact loading was conducted using a Split Hopkinson Pressure Bar (SHPB). In the single-impact tests, three driving pressures (0.35, 0.45, and 0.55 MPa) were applied to analyze the dynamic stress-strain response and energy absorption characteristics of concrete with different replacement ratios. In the cyclic impact tests, specimens were subjected to multiple impacts at a fixed pressure of 0.1 MPa until failure, to evaluate their damage evolution and accumulation characteristics under repeated low-energy impact loading. After impact, the fragmented specimens were subjected to standard sieving to obtain particle size distribution data, thereby comprehensively revealing the influence mechanism of CG content on the impact toughness and fragmentation characteristics of concrete.

Table 3. Experimental scheme

Original Number	Test Specimen ID	CG Replacement Ratio/%	Impact Mode	
			Impact Pressure/MPa	Number of Impacts
Single Impact	CG00-35	0	0.35	1
	CG00-45		0.45	
	CG00-55		0.55	
	CG15-35	15	0.35	1
	CG15-45		0.45	
	CG15-55		0.55	
	CG30-35	30	0.35	1
	CG30-45		0.45	
	CG30-55		0.55	
	CG45-35	45	0.35	1
	CG45-45		0.45	
	CG45-55		0.55	
Cyclic Impact	CG00-01X	0	0.1	Until failure
	CG15-01X	15		
	CG30-01X	30		
	CG45-01X	45		

3 Results and Discussion

3.1 Dynamic response characteristics of CGC under single impact

3.1.1 Evolution of dynamic mechanical properties of CGC

In SHPB impact tests, the uniform distribution of stress within the specimen is a crucial prerequisite for ensuring the validity of dynamic mechanical property testing. This study employed the "three-wave method" to verify the stress uniformity in CGC specimens during impact loading. This method involves analyzing the incident wave and reflected wave signals measured on the incident bar. Their superposition yields the stress history at the front end of the specimen, while the transmitted wave signal acquired on the transmission bar corresponds to the stress history at the rear end. By comparing the consistency between the transmitted wave curve and the superposition curve of the incident and reflected waves, the equilibrium state of internal stress within the specimen can be evaluated. The results show a good agreement between the two curves (Fig. 3), indicating that the internal stress state in the specimen was essentially uniform during loading. This satisfies the fundamental assumptions of the SHPB test, confirming the validity and reliability of the test data.

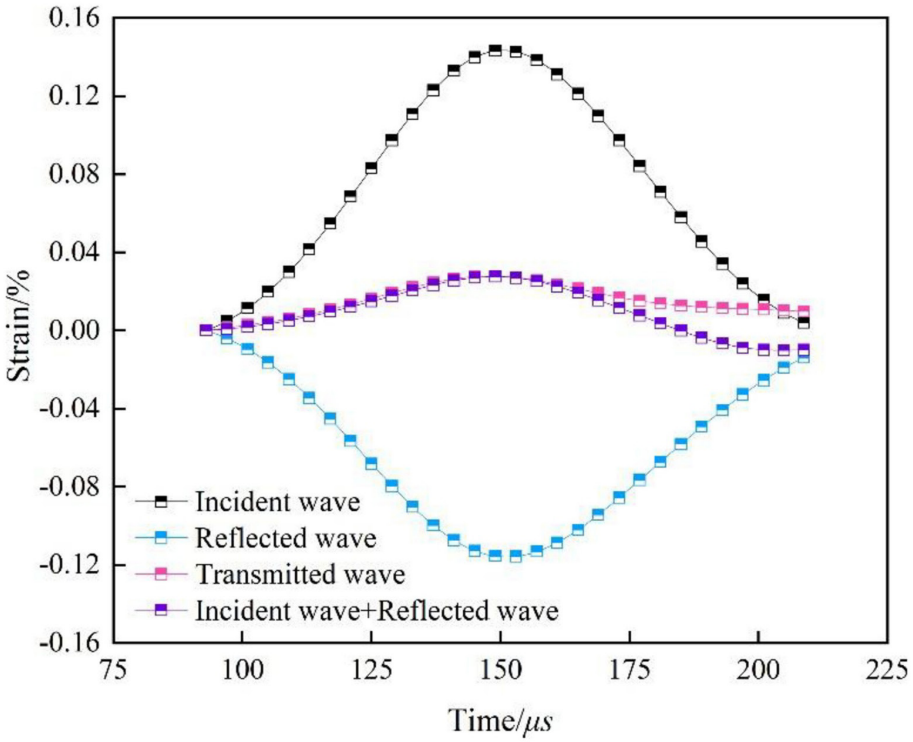

Figure 3. Three-wave equilibrium

When the striker impacts the free end of the incident bar, an incident wave $\varepsilon_i(t)$ is generated. As the incident wave reaches the interface between the specimen and the incident bar, part of it is reflected as a reflected wave $\varepsilon_r(t)$, while the remainder continues as a transmitted wave $\varepsilon_t(t)$ propagating into the transmission bar. Using the "three-wave method," the average stress σ_s, average strain $\varepsilon(t)$ and average strain rate $\dot{\varepsilon}(t)$,of the specimen can be determined. The corresponding formulas are as follows:

$$\sigma(t) = \frac{A_0}{2A_s} E\ [\varepsilon_i(t) + \varepsilon_r(t) + \varepsilon_t(t)] \tag{1}$$

$$\varepsilon(t) = \frac{C_o}{L_s} \int_0^t [\varepsilon_i(t) - \varepsilon_r(t) - \varepsilon_t(t)]dt \tag{2}$$

$$\dot{\varepsilon}(t) = \frac{C_o}{L_s}\left(\varepsilon_a(t) - \varepsilon_r(t) - \varepsilon_t(t)\right) \tag{3}$$

In the equations: $\varepsilon_i(t)$, $\varepsilon_r(t)$ and $\varepsilon_t(t)$ represent the incident, transmitted, and reflected strain signals in the bars, respectively. C_0 is the propagation velocity of the elastic wave in the bar, A_0 is the cross-sectional area of the steel pressure bar, E denotes the elastic modulus of the steel pressure bar, A_s is the cross-sectional area of the specimen, L_s is the length of the specimen.

Using the above formulas (1)– (3), the stress–strain curves of the specimens under single-impact loading were calculated, and the results are shown in Fig. 4.

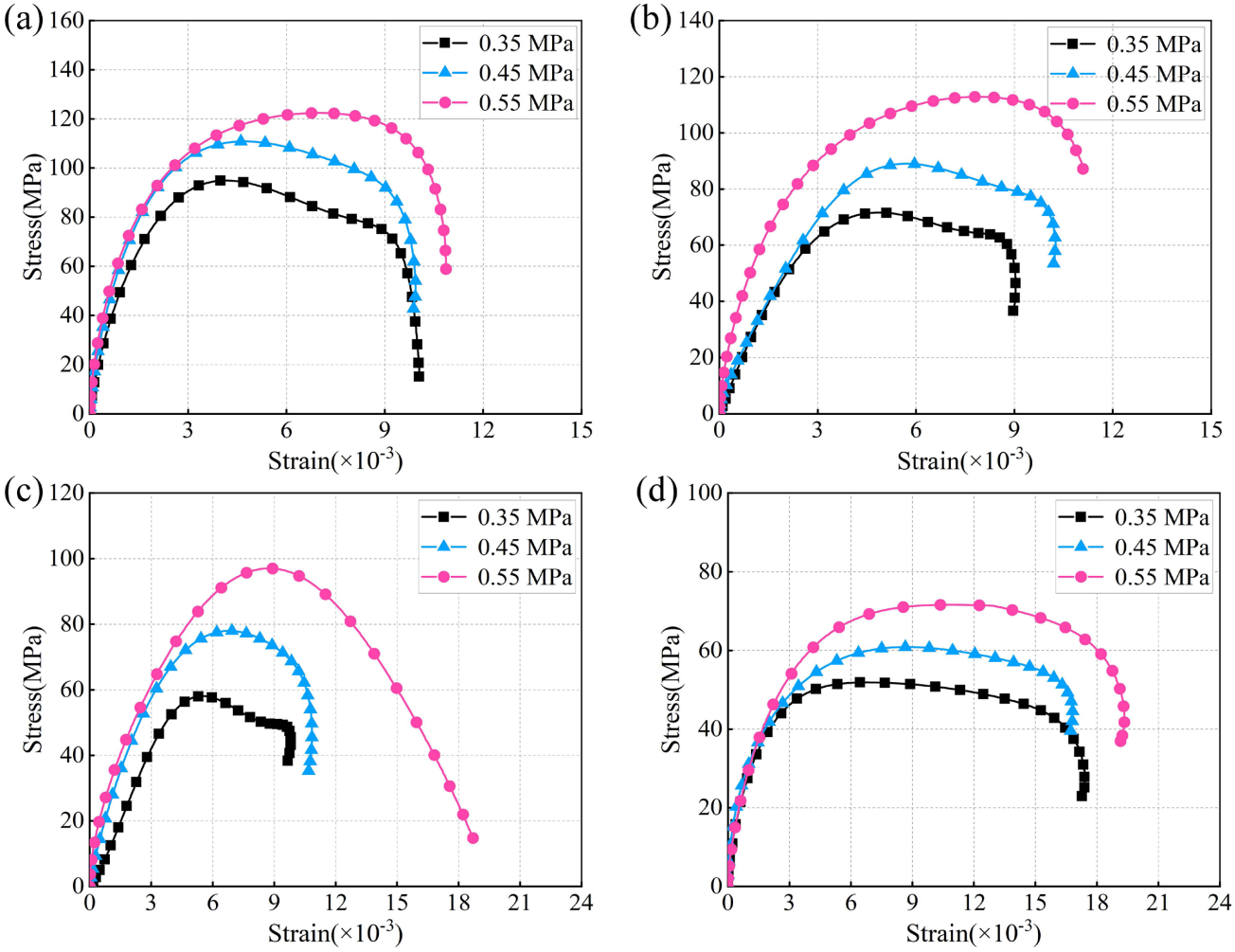

Figure 4. Stress-strain curves of specimens under single impact: **a** content 0%, **b** content 15%, **c** content 30%, **d** content 45%

Based on the information extracted from the aforementioned figures, the fundamental mechanical parameters of the rock were organized as shown in Table 4. The elastic modulus was taken as the secant slope at 50% of the peak strength (with reference). Furthermore, the variation trends of the mechanical properties of CGC under different replacement ratios were plotted, as shown in Fig. 5, to analyze the influence mechanism of CG content on the mechanical performance of concrete. According to the standards and suggested methods for rock-like materials and rock mechanics testing (Fairhurst & Hudson, 1999; Ministry of Geology and Mineral Resources of the PRC, 1995), elastic stiffness can be quantified using moduli defined by different conventions. Because the average elastic modulus is sensitive to the selected evaluation interval, it is prone to operator-dependent variability. Therefore, the deformation modulus is characterized using the secant modulus, defined as the slope of the line connecting the origin to the point at 50% of the peak stress on the stress–strain curve (Gong, 2010).

(a) Dynamic Compressive Strength

Fig. 5(a) shows the variation trend of the peak strength of CGC under single impact. Analysis reveals that under identical impact pressure, the dynamic strength of the specimen gradually decreases with increasing CG content. This trend is not affected by the magnitude of the impact pressure. Taking the 0.45 MPa impact pressure as an example, when the CG content is 0%, 15%, 30%, and 45%, the dynamic compressive strengths of the specimens are 110.82 MPa, 89.05 MPa, 77.98 MPa, and 60.86 MPa, respectively. These data indicate that as the CG content increases, the dynamic compressive strength of the specimen progressively declines, reflecting a gradual weakening of its resistance to impact failure.

Table 4. Basic information on mechanical properties under single impact

Impact Pressure (MPa)	CG Content (%)	Peak Strength (MPa)	Peak Strain(×10^{-3})	Elastic Modulus (GPa)
0.35 MPa	0	94.89	4.16	50.00
	15	71.63	4.87	24.97
	30	58.11	5.5	19.73
	45	51.91	6.81	13.99
0.45 MPa	0	110.82	4.72	56.06
	15	89.05	5.69	25.85
	30	77.98	6.79	20.22
	45	60.86	8.72	20.08
0.55 MPa	0	122.41	7.01	60.33
	15	112.88	7.89	38.81
	30	97.03	8.72	23.13
	45	71.61	10.73	24.38

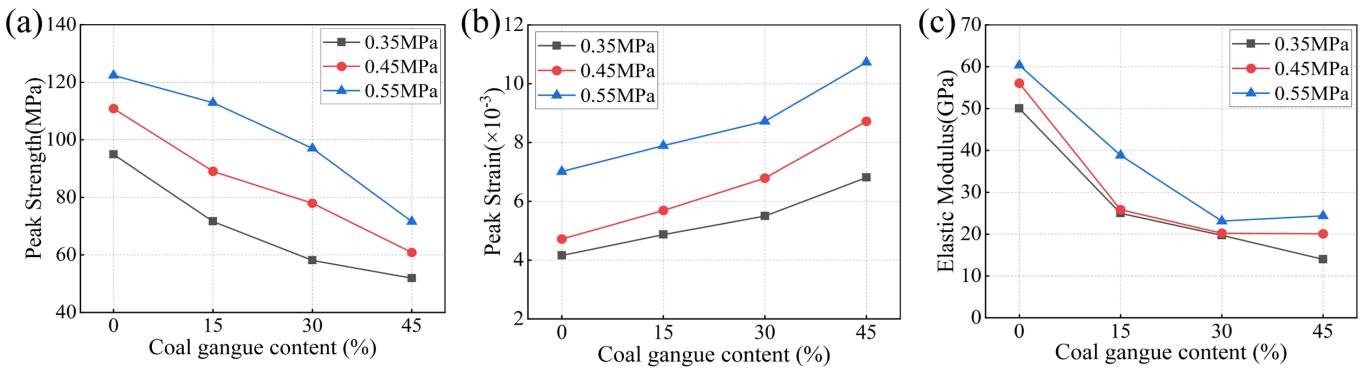

Figure 5. Evolution of mechanical properties of CGC under single impact: **a** peak strength, **b** peak strain, **c** elastic modulus

(b) Peak Strain

Further analysis was conducted on the strain value corresponding to the maximum dynamic stress reached by the specimens, as shown in Fig. 5(b). The results show that the strain required to reach peak stress increases gradually with higher CG content. Using the 0.45 MPa impact pressure as an example, the corresponding strain values for CG contents of 0%, 15%, 30%, and 45% are 0.00472, 0.00569, 0.00679, and 0.00872, respectively. Data processing reveals that during the increase in CG content from 0% to 45%, the strain increments are 0.00097, 0.00110, and 0.00193, respectively. It is noteworthy that when the CG content increases from 30% to 45%, the strain increment rises significantly. This indicates that as the CG content increases, the specimen's resistance to deformation before peak stress gradually weakens. Furthermore, after the CG content reaches a certain critical level, its deformation resistance deteriorates sharply.

(c) Elastic Modulus

Fig. 5(a) shows the variation trend of the elastic modulus of CGC under single impact. The experimental data indicate a significant negative correlation between CG content and the concrete's elastic modulus, meaning the material's elastic modulus exhibits a monotonic decreasing trend with increasing content, signifying a systematic degradation of its stiffness. Specifically, under a 0.35 MPa impact pressure, the elastic modulus drastically decreases from 50.00 GPa for the reference group (0% content) to 13.99 GPa at 45% content. This pattern holds consistently across different energy levels; for instance, under 0.45 MPa and 0.55 MPa conditions, the elastic moduli also decrease from 56.06 GPa and 60.33 GPa to 20.08 GPa and 24.38 GPa, respectively. It is noteworthy that higher impact energy (e.g., 0.55 MPa) exhibits a certain buffering effect on the decline of elastic modulus in the high-content range (30%-45%), manifested as a slowing rate of decrease or even a slight rebound. However, this does not alter the overall content-dominated trend of stiffness degradation.

The dynamic mechanical properties of CGC are jointly regulated by impact pressure and CG content. Increasing the impact pressure strengthens the material through strain rate effects, manifested as improvements in strength, elastic modulus, and peak strain. Conversely, increasing CG content introduces brittle weak interfaces, leading to significant degradation in strength and stiffness. It is noteworthy that although CG reduces stiffness, it enhances energy dissipation through particle slip and crushing, resulting in larger strain at failure, reflecting a transition in failure mode towards greater ductility.

This mechanistic understanding holds significant guiding importance for engineering practice: In engineering sections where stress bearing is the primary concern, the material characteristics of CG can be appropriately utilized. In areas requiring strict deformation control, its usage should be limited. By optimizing the material mix ratio, a balance between load-bearing capacity and deformation control can be achieved.

3.1.2 Energy dissipation mechanism and fragmentation characteristics of CGC

(a) Evolution of energy absorption capacity of CGC with different gangue contents

Energy absorption is a key indicator characterizing a material's dynamic impact resistance. The energy evolution law of concrete under impact loading is characterized by calculating the area under the stress-strain curve before the peak, thereby elucidating the influence mechanism of different CG contents on its dynamic damage process and failure mode. As shown in Table 5, the energy absorption of specimens under single impact is presented.

Table 5. Energy absorption capacity of CGC under single impact (MJ/m^3)

Impact Pressure	CG Content			
	0%	15%	30%	45%
0.35 MPa	0.2899	0.2388	0.1922	0.2876
0.45 MPa	0.4021	0.3406	0.3710	0.3710
0.55 MPa	0.4307	0.6933	0.6016	0.6223

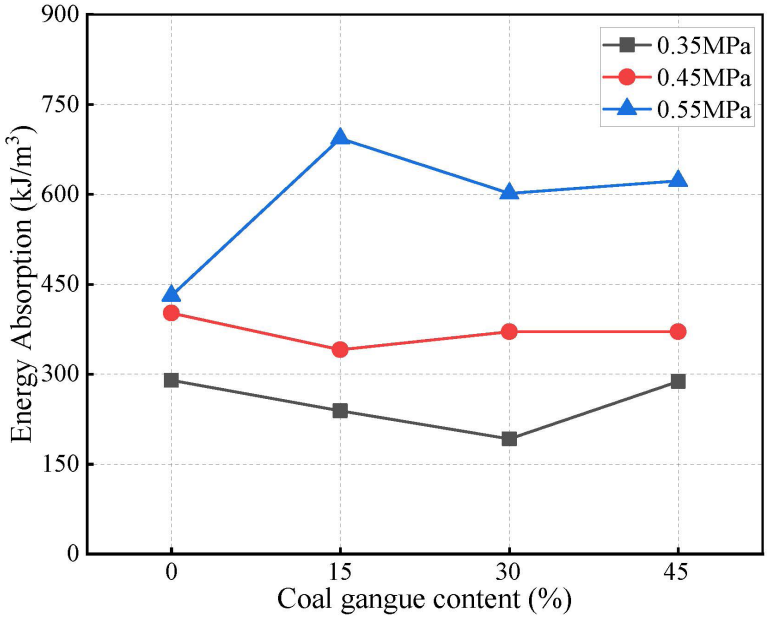

Figure 6. Energy absorption curves of CGC under single impact

As shown in Fig. 6, the impact pressure is the decisive external factor controlling the energy absorption level of the specimens. Under all CG content conditions, the absorbed energy of the specimens increases significantly as the impact pressure rises from 0.35 MPa to 0.55 MPa. This suggests that an increase in the intensity of the external dynamic load is the fundamental driver of dynamic disasters in coal-rock masses. In engineering practice, this corresponds to high-energy dynamic loads generated by factors such as increased mining depth and the fracturing of hard roof strata.

Secondly, the influence of CG content on the energy absorption capacity of the specimens exhibits significant nonlinear characteristics. In the low to medium CG content range, the overall trend of energy absorption is decreasing. This stems from the fact that gangue particles disrupt the integrity of the coal matrix, becoming points of stress concentration and preferential sites for crack propagation, thereby weakening the overall strength and elastic energy storage capacity of the specimen. However, when the CG content increases to a higher level, the absorbed energy shows a rebound. This indicates that the material's mechanical properties become dominated by the gangue skeleton, and the energy absorption mechanism shifts from being primarily elastic energy storage to dissipation processes dominated by inter-particle friction, crushing, and plastic flow.

(b) Fragmentation distribution characteristics of CGC with different gangue contents

Table 6 systematically presents the failure modes of concrete with different CG contents under single impact. Analysis reveals that the degree of specimen damage shows a significant positive correlation with both impact pressure and CG content. Specifically: 1) At a fixed CG content, as the impact pressure increases from 0.35 MPa to 0.55 MPa, the failure mode of the specimen evolves from localized crushing or the development of a single main crack to multi-crack propagation, coalescence, and even complete fragmentation, reflecting the decisive role of external impact energy input on material damage. 2) Under the same impact pressure, as the CG content increases from 0% to 45%, the overall integrity and toughness of the specimen decrease significantly. The failure mode progresses from controlled brittle cracking to comprehensive fragmentation, indicating that gangue, as an internal defect, effectively reduces the material's fracture energy and accelerates the damage accumulation process. Notably, under the condition of 45% CG content and 0.55 MPa impact pressure, the specimen is nearly completely disintegrated, resulting in a total loss of structural load-bearing capacity.

Table 6. Failure modes of specimens under single impact

Impact Pressure	CG Content			
	0%	15%	30%	45%
0.35 MPa				
0.45 MPa				
0.55 MPa				

Fig. 7 quantitatively reveals the synergistic effects of impact pressure and CG content on the fragmentation characteristics of CGC through the mass fraction distribution of concrete fragments. Analysis indicates that with increasing impact pressure or CG content, the particle distribution exhibits a significant trend toward finer fragmentation. Specifically, the proportion of larger particles (e.g., >20 mm) decreases, while the proportion of smaller particles (e.g., 10–20 mm) increases. This pattern confirms that higher external energy input and greater internal defects collectively promote a more thorough fragmentation process. Notably, under the conditions of 45% CG content and 0.55 MPa impact pressure, the particle distribution is highly concentrated in the smaller size ranges. This signifies a transition in the fragmentation mode from localized splitting to overall crushing.

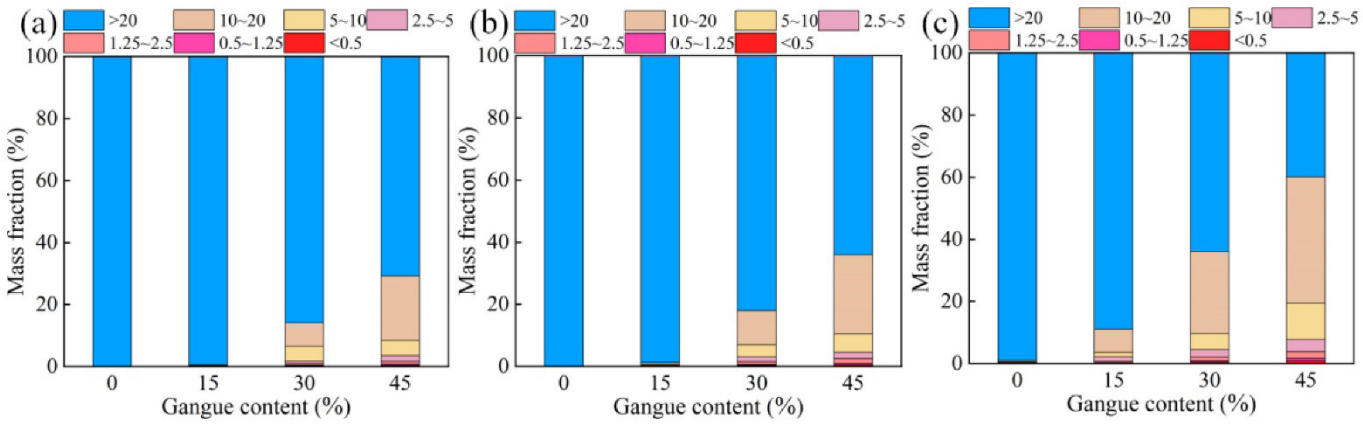

Figure 7. Particle size distribution of specimen fragmentation under single impact: **a** impact gas pressure 0.35 MPa, **b** impact pressure 0.45 MPa, **c** impact pressure 0.55 MPa

3.2 Evolution of cumulative damage in mechanical properties under cyclic impact

By conducting single-impact tests on CGC with varying contents under different impact pressures, the influence mechanism of CG content on the dynamic mechanical properties, energy dissipation mechanisms, and impact fragmentation characteristics of CGC was elucidated. It was found that both high-energy impact and CG content significantly affect the dynamic mechanical properties of concrete. Furthermore, in addition to high-energy single dynamic loads, repeated low-energy dynamic loads are also frequently encountered in the surrounding rock of underground coal mine roadways. The action of repeated dynamic loads typically leads to cumulative damage, degradation of mechanical properties, and even structural instability in the roadway surrounding rock mass. Therefore, to investigate the damage accumulation and performance degradation laws of CGC under repeated low-energy dynamic loads, cyclic impact tests on CGC were conducted.

3.2.1 Degradation laws of mechanical properties of CGC under repeated impact

CGC specimens were subjected to cyclic impact loading at a constant impact pressure of 0.1 MPa. Using formulas (1)– (3), the stress-strain curves for each impact under repeated loading were obtained, as shown in Fig. 8.

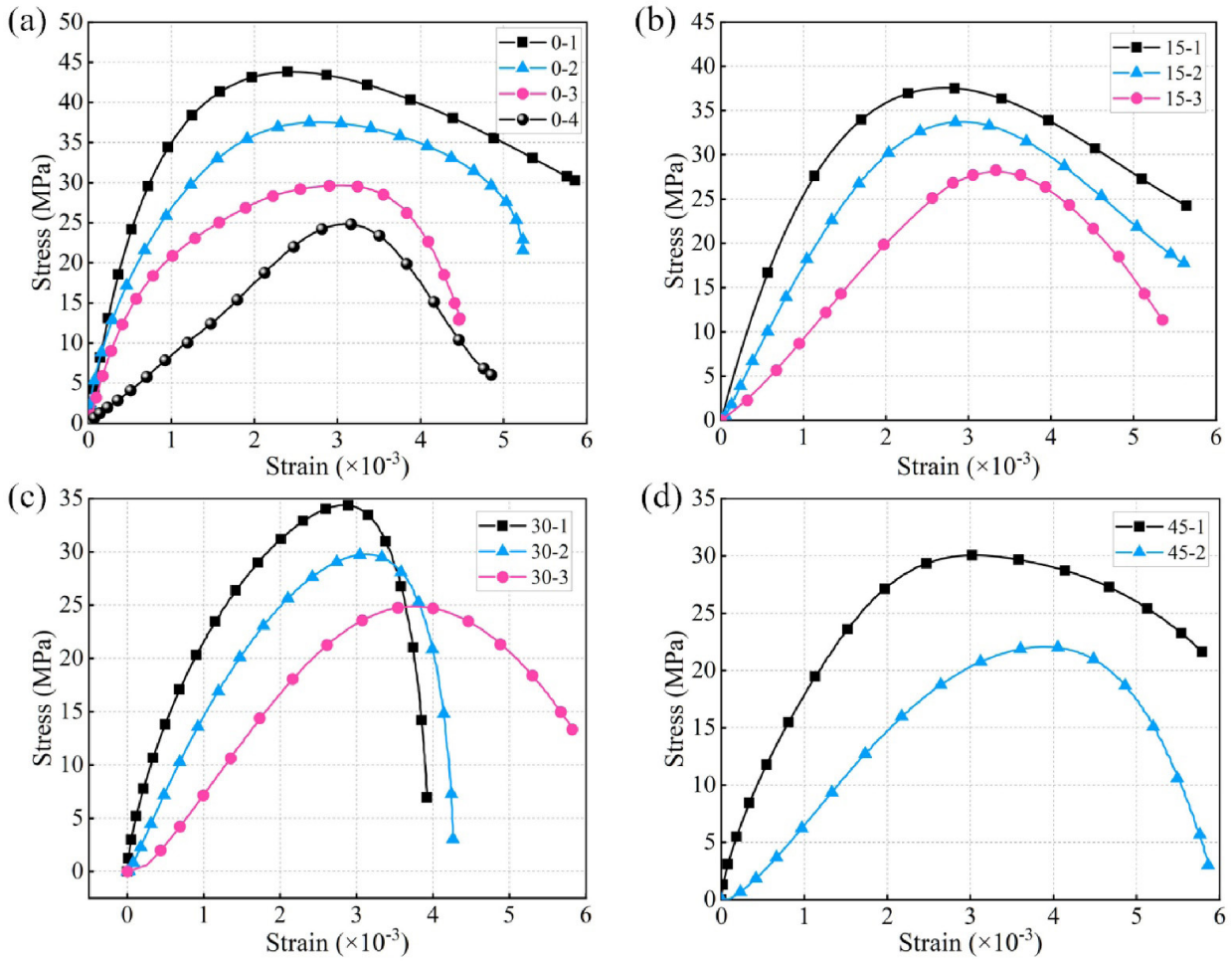

Figure 8. Stress-Strain Curves of CGC under Cyclic Impact: **a** CG Content 0%, **b** CG Content 15%, **c** CG Content 30%, **d** CG Content 45%

The peak strength and peak strain after each impact are extracted from Fig. 8, while the elastic modulus and rock damage degree are calculated. The method for calculating the elastic modulus in the multiple impact experiments is the same as that used for the single impact tests. The damage degree is calculated using a cumulative approach. The formula for the damage caused by a single impact is: $D_n = E_{(n-1)} / E_n$,The formula for cumulative calculation is:

$$D_{\Sigma n} = \begin{cases} 0 & (n=1) \\ D_{(n\text{-}1)} + D_n(1\text{-}D_{\Sigma(n\text{-}1)}) & (n>1) \end{cases} \tag{4}$$

The experimentally extracted and calculated data are summarized in Table 7. The evolution laws of the mechanical properties of CGC under cyclic impact are illustrated in Fig. 9.

Table 7. Mechanical properties of CGC under cyclic impact

CG Content (%)	Number of Impacts	Peak Strength (MPa)	Peak Strain (×10^{-3})	Elastic Modulus (GPa)
0	1	43.80	2.45	40.21
	2	37.53	2.77	28.30
	3	32.35	3.04	22.01
	4	24.83	3.10	8.54
15	1	37.68	2.72	27.80
	2	33.86	3.23	18.43
	3	28.34	3.33	10.21
30	1	34.38	2.84	22.30
	2	29.75	3.11	14.44
	3	24.88	3.75	8.34
45	1	30.05	3.05	19.40
	2	22.07	3.90	7.20

The results indicate that under low-pressure cyclic impact conditions, the impact resistance of CGC shows a trend of initial gradual decline followed by a sharp drop as the CG replacement ratio increases. The experimental data show that when the CG replacement ratios are 0%, 15%, 30%, and 45%, the corresponding number of impacts the specimens can withstand are 4, 3, 3, and 2, respectively. This pattern can be explained as follows: at moderate replacement ratios (15%–30%), although CG introduces a certain degree of strength loss, it acts as an energy dissipation medium. Through inter-particle friction and localized micro-fracturing, it can absorb impact energy, thereby preventing a significant reduction in the number of sustained impacts. However, when the replacement ratio increases to 45%, the excessive weak interfaces severely compromise the overall integrity of the material, leading to rapid structural instability and failure under impact loading.

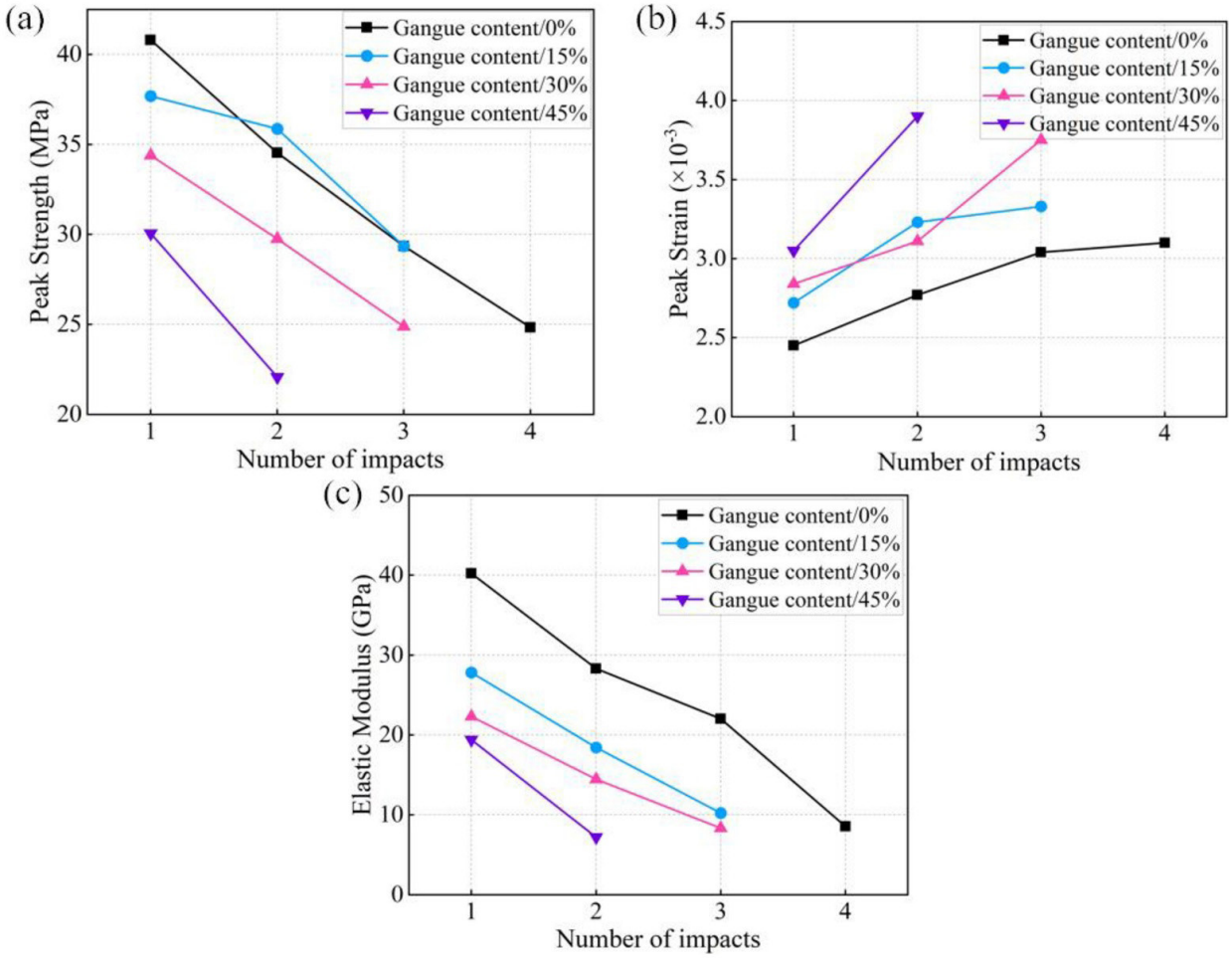

Figure 9. Evolution of mechanical properties of CGC under cyclic impact: **a** peak strength, **b** peak strain, **c** elastic modulus

Fig. 9 data show that under low-energy cyclic impact, the mechanical properties of CGC exhibit a regular evolution pattern. As the number of impacts increases, the peak strength and elastic modulus of the specimens continuously decrease, while the peak strain correspondingly increases. This change aligns with the "weak-phase-dominated" mechanism in composite materials: CG, as a brittle inclusion phase, reduces the load-bearing capacity and stiffness of the material by introducing numerous weak interfaces. Simultaneously, the relative displacement and fragmentation processes between its particles provide additional inelastic deformation, promoting a shift in the material's failure mode from brittle to ductile.

From a mesoscopic mechanism perspective, the aforementioned performance degradation stems from the gradual accumulation of internal damage. During the impact process, microcracks undergo stages of initiation, propagation, and coalescence, leading to two macroscopic responses: the continuous increase in peak strain reflects the reduction in the effective load-bearing area, exhibiting a "deformation-hardening" characteristic; the decrease in elastic modulus corresponds to stiffness degradation, essentially resulting from the increase in inelastic deformation components caused by defects such as microcracks, which reduces the slope of the stress-strain curve. The CG replacement ratio has a critical influence on this damage evolution, with specimens of different replacement ratios showing varying rates of damage development and final failure morphology.

In summary, a higher CG replacement ratio leads to more significant degradation of mechanical properties under cyclic impact. Increasing the replacement ratio accelerates stiffness degradation and damage accumulation, thereby reducing impact resistance. This pattern indicates that the gangue replacement ratio directly affects the material's dynamic durability: when the replacement ratio does not exceed 30%, the material retains a certain level of impact resistance; when the replacement ratio increases to 45%, the fatigue damage process significantly accelerates, severely undermining its applicability and support effectiveness in engineering.

3.2.2 Evolution of energy absorption capacity of CGC under repeated impact

To investigate the influence of CG as a replacement aggregate on the dynamic energy absorption characteristics of concrete, the energy absorption data of specimens under cyclic impact were obtained by calculating the area under the dynamic stress-strain curve before the peak (Table 8). Based on this data, the evolution of energy absorption capacity during the impact process was systematically analyzed, thereby revealing the influence mechanism of gangue replacement ratio on the dynamic damage accumulation and failure mode of concrete.

Table 8. Energy absorption characteristics of CGC under cyclic impact (MJ/m^3)

Gangue content (%)	Number of d impacts				Cumulative
	1st Impact	2nd Impact	3rd Impact	4th Impact	
0	0.0757	0.0715	0.0667	0.0413	0.2552
15	0.0726	0.0671	0.0545		0.1942
30	0.0679	0.0586	0.0535		0.1801
45	0.0644	0.0506			0.1151

Further analysis of the data in Table 8 reveals the evolution patterns of single-impact energy absorption and cumulative energy absorption of CGC under cyclic impact, as shown in Fig. 10.

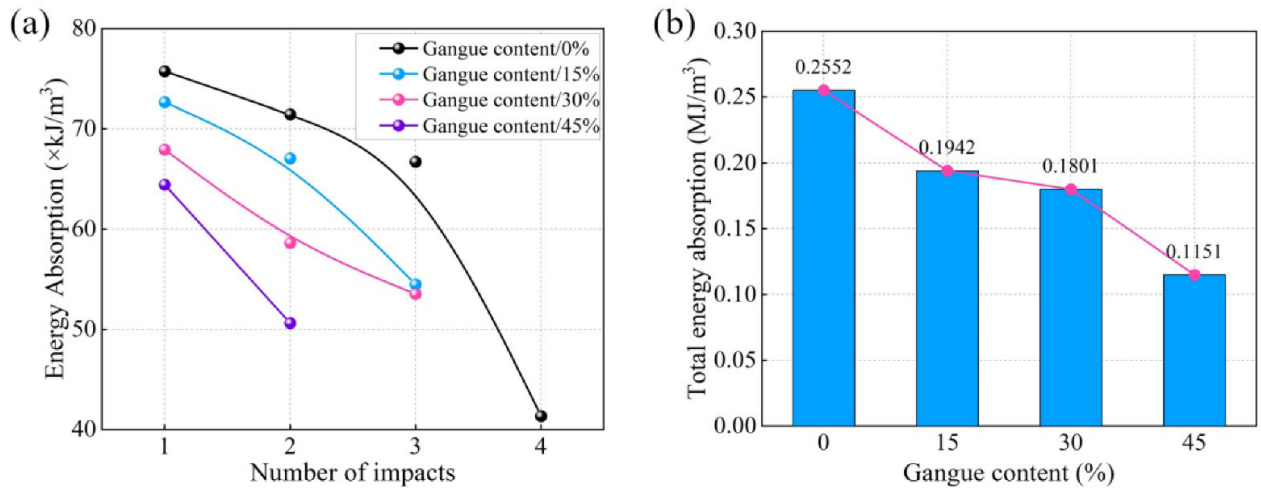

Figure 10. Energy absorbed of CGC under cyclic impact: **a** energy absorbed per impact, **b** total energy absorbed

Fig. 10(a) shows the evolution of single-impact energy absorption for all specimens. The overall trend indicates a progressive decrease in absorbed energy with increasing impact number, characterizing the damage accumulation process due to the initiation, propagation, and coalescence of internal microcracks under cyclic impact loading. For the specimen with 0% CG content, failure occurred after 4 impacts. The energy absorption decreased from 0.0757 MJ/m^3 in the first impact to 0.0413 MJ/m^3 just before failure, with a relatively gradual decline in the first three impacts (0.0715 and 0.0667 MJ/m^3 in the second and third, respectively) followed by a sharp drop in the final impact. This suggests an abrupt damage evolution near the critical point. Moreover, as the CG replacement ratio increases, both the initial absorbed energy and the resistance to cyclic impacts deteriorate. Specifically, the first-impact energy absorption decreased from 0.0757 MJ/m^3 at 0% CG to 0.0644 MJ/m^3 at 45% CG. Concurrently, the rate of energy decay accelerated. Under the high replacement ratio of 45%, the specimen failed after only two impacts, with the absorbed energy in the second impact (0.0506 MJ/m^3) showing a significant reduction compared to the first. This behavior reflects that the relatively weak interfacial transition zone between CG and the concrete matrix acts as a potential stress concentrator, promoting rapid damage development and unstable crack propagation.

As shown in Fig. 10(b), the total absorbed energy of the specimens with different CG contents exhibited significant differences. Specifically, specimens with CG contents of 0%, 15%, 30%, and 45% showed cumulative absorbed energies before failure of 0.2552 MJ/m^3, 0.1942 MJ/m^3, 0.1801 MJ/m^3, and 0.1151 MJ/m^3, respectively. The energy absorption capacity of the material showed a gradual decreasing trend with increasing CG content. As the CG content increased from 0% to 45%, the total energy dissipation capacity decreased by approximately 54.9%. The simultaneous decline in total energy absorption level and impact life collectively indicates that increasing the CG replacement ratio systematically degrades the concrete's toughness, energy dissipation capacity, and damage tolerance under dynamic loading.

In summary, increasing the CG replacement ratio systematically degrades the dynamic impact resistance of the concrete material. This is specifically manifested as a reduction in single-impact energy absorption level, an acceleration of the damage evolution rate, and a significant decline in both overall energy absorption capacity and cyclic impact life.

Table 9. Failure modes of specimens under cyclic impact

Impact Pressure	CG Content			
	0%	15%	30%	45%
0.1Mpa Cyclic Impact		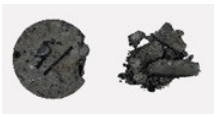	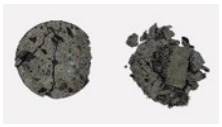	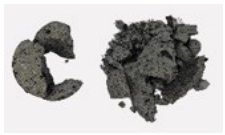

As shown in Table 9, with increasing CG content, the fragmentation degree of the specimens under impact loading is significantly intensified, and the failure morphology changes markedly. When the CG content is 0%, the specimens exhibit quasi-static failure characteristics with localized spalling. In contrast, when the CG content increases to 45%, the specimens are completely disintegrated into fragments. Quantitative analysis of the particle size distribution of the CGC fragments after impact reveals that as the CG content increases, the proportion of larger fragments significantly decreases under cyclic impact, and the particle size distribution becomes more concentrated in the smaller size ranges (Fig. 11).

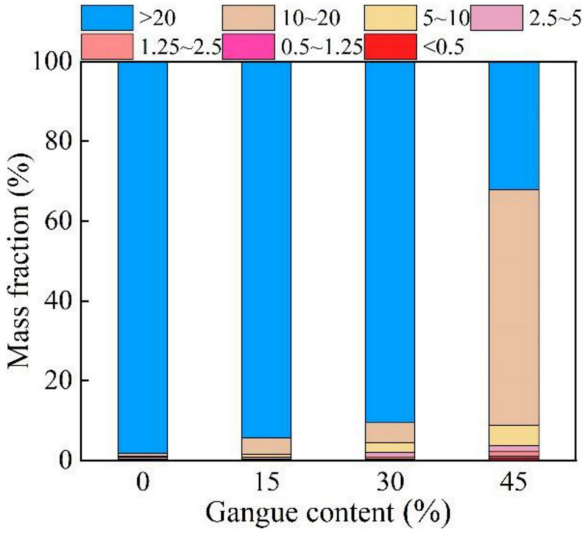

Figure 11. Mass distribution of specimens subjected to 0.1 MPa cyclic impact

3.3. Impact Failure Mechanism and Performance Degradation Model of CGC

The preceding experiments have clarified the synergistic influence of impact pressure and CG replacement ratio on the dynamic performance of CGC: impact pressure enhances material strength through the strain rate effect, while the CG replacement ratio systematically degrades its stiffness and integrity by introducing weak interfaces. At higher replacement ratios, it further shifts the energy absorption mechanism from elastic storage to dissipative processes such as friction and crushing. These phenomena collectively reveal the "weak-phase-dominated" damage evolution characteristic of the material under dynamic loading.

3.3.1 Impact failure mechanism of CGC

The impact failure of CGC originates from its internally formed heterogeneous composite structure. The altered interface properties and the inherent performance differences of the aggregate jointly constitute the core of its performance evolution. On one hand, the surface of CG aggregate is rough, porous, and exhibits weaker chemical bonding with the cement paste. This results in a more significant disparity in the elastic modulus, wave impedance, and bonding strength of the interfacial transition zone (ITZ) between the aggregate and the matrix compared to that of ordinary crushed stone aggregate. Under impact loading, these inherently weak interfaces become preferential regions for stress wave reflection, refraction, and stress concentration, thereby significantly promoting the initiation of microcracks, as shown in Fig. 12.

On the other hand, the mechanical properties of CG aggregate itself are typically markedly inferior to those of natural crushed stone—it has lower strength and greater brittleness, making it more prone to fragmentation under stress. Consequently, during the impact process, not only is the interfacial zone susceptible to damage, but the CG aggregate itself also acts as a "soft spot" within the material, further exacerbating the non-uniformity of stress distribution and the accumulation of damage.

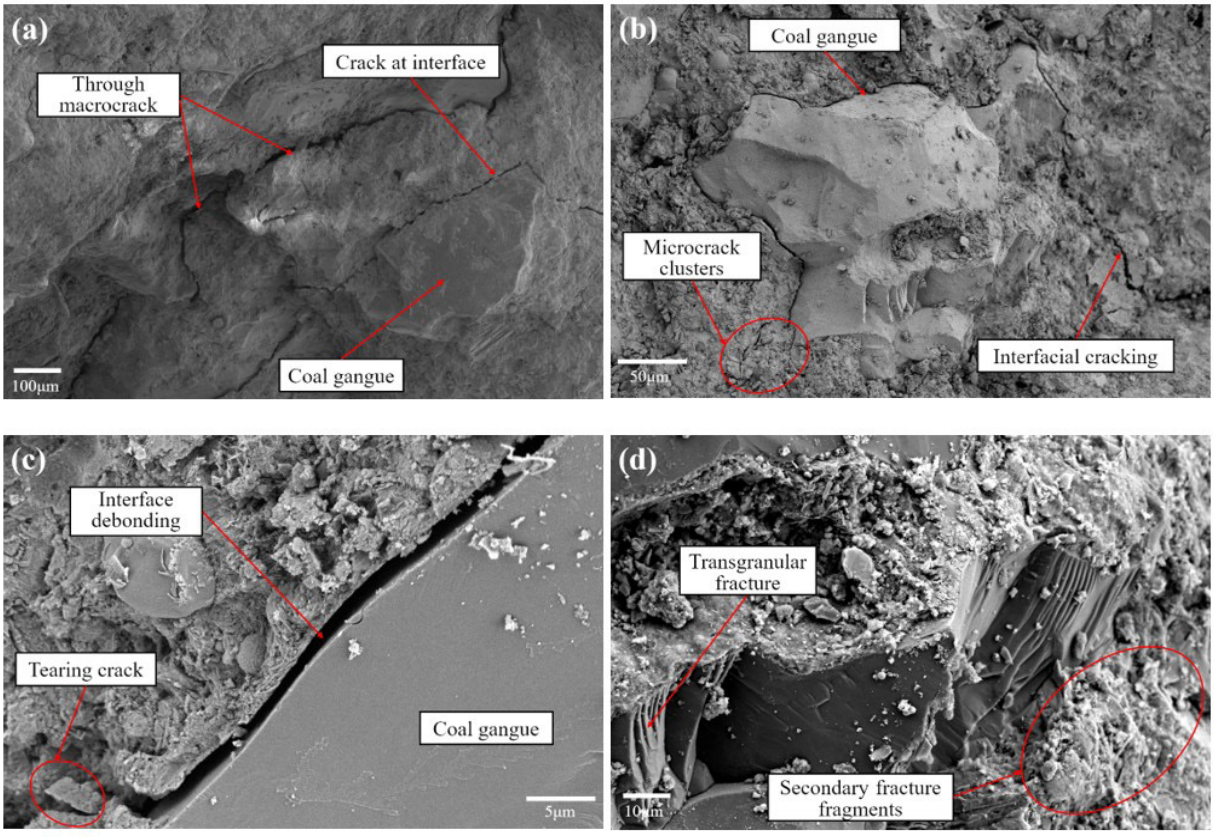

Figure 12. Microstructure of typical specimens: **a** lateral crack propagation along CG (×100), **b** peripheral crack development around CG (×300), **c** debonding at the cg–matrix interface (×3000), **d** fracture morphology of CG (×1000)

As the CG replacement ratio increases, although the total mass of coarse aggregate remains unchanged, the effective proportion of "weak interfaces" and "low-strength aggregate" per unit volume rises significantly. This is because the relatively poor-performing CG–matrix interface progressively replaces the better-performing crushed stone–matrix interface, while low-strength CG particles also substitute for high-strength crushed stone particles. Consequently, even in the early stages of loading, the material experiences simultaneous interface debonding and aggregate fracture at multiple locations, which manifests macroscopically as a systematic degradation of dynamic strength and elastic modulus with increasing CG replacement ratio.

The dynamic failure mode of the material therefore undergoes a systematic evolution: At low replacement ratios, failure is still governed by the dominant, relatively continuous system of the matrix and crushed stone interfaces, where the aggregates themselves possess higher strength, resulting overall in quasibrittle fracture. At medium to high replacement ratios, the coexistence of numerous weak interfaces and lowstrength aggregates leads to the simultaneous initiation and rapid interconnection of microcracks at multiple sites, forming a distributed damage network, and aggregate fragmentation becomes increasingly pronounced. When the replacement ratio reaches high levels such as 45%, the mechanical behavior is entirely dominated by the “CG skeleton” and its weak interfaces. Aggregate selffragmentation and interparticle frictional slip become the primary energydissipation mechanisms, leading macroscopically to a more thorough crushingtype failure. The impact energyabsorption mechanism also transforms accordingly: At low replacement ratios, elastic energy storage predominates; at high replacement ratios, impact energy is mainly consumed through plastic dissipation processes such as frictional slip at numerous weak interfaces and particle crushing. This explains the plateau behavior observed in the stressstrain curves of highreplacementratio specimens and the occasional recovery of energyabsorption values under specific conditions.

3.3.2 Impact performance degradation model of CGC

The degradation of the mechanical properties of CGC under cyclic impact loading is a complex physical process, involving primarily the following damage mechanisms: impact energy induces the generation of microcracks within the material, which propagate with increasing numbers of impacts; the interface between the CG aggregate and the cement paste undergoes debonding under impact; and the impact loading causes changes in the internal pore structure of the material, affecting its overall strength.

To characterize the law of dynamic strength degradation, based on the theory of damage mechanics, an exponential-form dynamic strength degradation model was selected. This model effectively describes the cumulative damage behavior of materials under cyclic loading. The basic form of the model expresses the dynamic strength $\sigma_d\ (N,C)$ as the product of the initial dynamic strength function $\sigma_{d0}(C)$ and the relative strength retention rate function $R_\sigma(N,C)$. Here, $\sigma_d\ (N,C)$ represents the dynamic strength after *N* impacts with a CG content of *C*:

$$\sigma_d\ (N,C)=\sigma_{d0}\ (C)\cdot R_\sigma(N,C) \tag{5}$$

where $\sigma_{d0}(C)$ is the initial dynamic strength function related to the CG content, and $R_\sigma(N,C)$ denotes the strength retention rate after *N* impacts.

First, the initial strength function $\sigma_{d0}\ (C)$ was determined. Using the experimental data points for *N*=0(C=0%, 58.2MPa;C=15%,53.5MPa;C=30%,44.3MPa;C=45%,37.7MPa), linear regression analysis via the least squares method yielded:

$$\sigma_{d0}\ (C)=58.2-0.456C \tag{6}$$

The goodness-of-fit for this linear approximation is R^2=0.998, indicating a significant linear negative correlation between the initial dynamic strength and the CG content.

Next, the relative strength degradation function $R_\sigma(N,C)$ was established. An exponential-form degradation function was adopted:

$$R_\sigma(N,C)=\exp\left[-\left(\frac{N}{\alpha(C)}\right)^{\beta(C)}\right] \tag{7}$$

where $\alpha(C)$ and $\beta(C)$ are material parameters related to the CG content *C*. $\alpha(C)$:Scale parameter, reflecting the characteristic impact life of the material. $\beta(C)$:Shape parameter, describing the dispersion of damage accumulation.

To calculate the relative strength, R_σ is defined as $R_\sigma=\sigma_d\ (N,C)/\sigma_0\ (C)$. The relative strength values for each condition were calculated based on the experimental data, as shown in Table 10.

Table 10. Calculation results of relative strength retention rate

	CG Content C (%)															
	0					15				30				45		
N	0	1	2	3	4	0	1	2	3	0	1	2	3	0	1	2
R_σ	1.00	0.75	0.65	0.56	0.43	1.00	0.70	0.63	0.53	1.00	0.78	0.67	0.56	1.00	0.80	0.59

To fit the parameters $\alpha(C)$ and $\beta(C)$, take the natural logarithm twice on both sides of the exponential model to obtain the linear form:

$$\ln(-\ln R_\sigma) = \beta(C)\cdot \ln N - \beta(C)\cdot \ln \alpha(C) \tag{8}$$

Let $Y = \ln(-\ln R_\sigma)$, $X = \ln N$ then the equation transforms into:

$$Y = \beta(C)\cdot X - \beta(C)\cdot \ln \alpha(C) \tag{9}$$

Through systematic parameter fitting and optimization, the values of $\alpha(C)$ and $\beta(C)$ for different CG contents were obtained. Table 11 presents the model parameters and the goodness of fit corresponding to each CG content:

Table 11. Fitting results of model parameters for different CG contents

C (%)	α(*C*)	β(*C*)	R^2
0	6.800	0.720	0.96
15	5.892	0.833	0.96
30	4.955	0.895	0.98
45	4.119	0.935	0.99

Further analysis of the relationship between the parameters $\alpha(C)$ and $\beta(C)$ and the CG content *C* reveals that these two parameters exhibit certain regularities with variations in *C*. To establish a unified predictive model, the specific forms of the parameter functions were obtained through regression analysis.

$\alpha(C)$ is a scale parameter reflecting the characteristic impact life of the material. Based on experimental data, it was found that $\alpha(C)$ first increases and then decreases with increasing CG content, reflecting the complex influence of CG on the impact performance of concrete. A rational function form was used to describe $\alpha(C)$:

$$\alpha(C) = \frac{6.8 + 0.05C}{1 + 0.015C + 0.00025C^2} \tag{10}$$

When *C*=0, $\alpha(0)$=6.8, corresponding to the characteristic impact life of plain concrete. The numerator term 6.8+0.05*C* reflects the initial strengthening effect of CG. The denominator term 1+0.015C+0.00025C^2 describes the negative impact of increasing CG content on the impact life. The parameters were optimized using the nonlinear least squares method to ensure the best fit with the experimental data at all CG content levels.

$\beta(C)$ is a shape parameter describing the dispersion of damage accumulation. As the CG content increases, the inhomogeneity of the material increases, and the dispersion of damage accumulation also changes accordingly. An exponential saturation function was used to describe $\beta(C)$:

$$\beta(C) = 0.72 + 0.25\left(1 - e^{-0.04C}\right) \tag{11}$$

When *C*=0, $\beta(0)$=0.72, corresponding to the damage accumulation characteristics of plain concrete. As *C* increases, $\beta(C)$ gradually approaches 0.97, reflecting the inhomogeneity introduced by CG. The exponential term 1-e^-0.04censures a smooth transition of the function, avoiding abrupt changes.

Integrating the above analyses, the complete model for predicting the dynamic strength of CGC under cyclic impact is obtained:

$$\sigma_d(N,C) = (58.2 - 0.456C)\cdot \exp\left[-\left(\frac{N}{\frac{6.8 + 0.05C}{1 + 0.015C + 0.00025C^2}}\right)^{0.72+0.25\left(1-e^{-0.04C}\right)}\right] \tag{12}$$

To verify the model's accuracy, it was used to calculate the predicted dynamic strength values for all experimental conditions. A comparison with the experimental values is presented in Table 12.

Table 12. Comparison of model predicted values and experimental values

C (%)	N	Experimental Value (MPa)	Predicted Value (MPa)	Absolute Error (MPa)	Relative Error (%)
0	0	58.20	58.20	0.00	0.00
0	1	43.80	45.26	1.46	3.33
0	2	37.53	38.46	0.93	2.48
0	3	32.35	33.42	1.07	3.31
0	4	24.83	29.41	4.58	18.45
15	0	53.50	51.36	-2.14	-4.00
15	1	37.68	40.88	3.20	8.49
15	2	33.86	34.20	0.34	1.00
15	3	28.34	29.05	0.71	2.51
30	0	44.30	44.52	0.22	0.50
30	1	34.38	35.06	0.68	1.98
30	2	29.75	28.56	-1.19	-4.00
30	3	24.88	23.52	-1.36	-5.47
45	0	37.70	37.68	-0.02	-0.05
45	1	30.05	28.86	-1.19	-3.96
45	2	22.07	22.68	0.61	2.76

The model accuracy evaluation, as shown in Fig. 13, indicates an overall mean absolute error of 1.23 MPa and a mean relative error of 3.89%. The maximum absolute error is 3.56 MPa, with over 81% of the predicted values exhibiting a relative error of less than 4%. This model accurately captures the dynamic strength degradation law of CGC under cyclic impact, providing a theoretical basis for safety assessment in engineering applications.

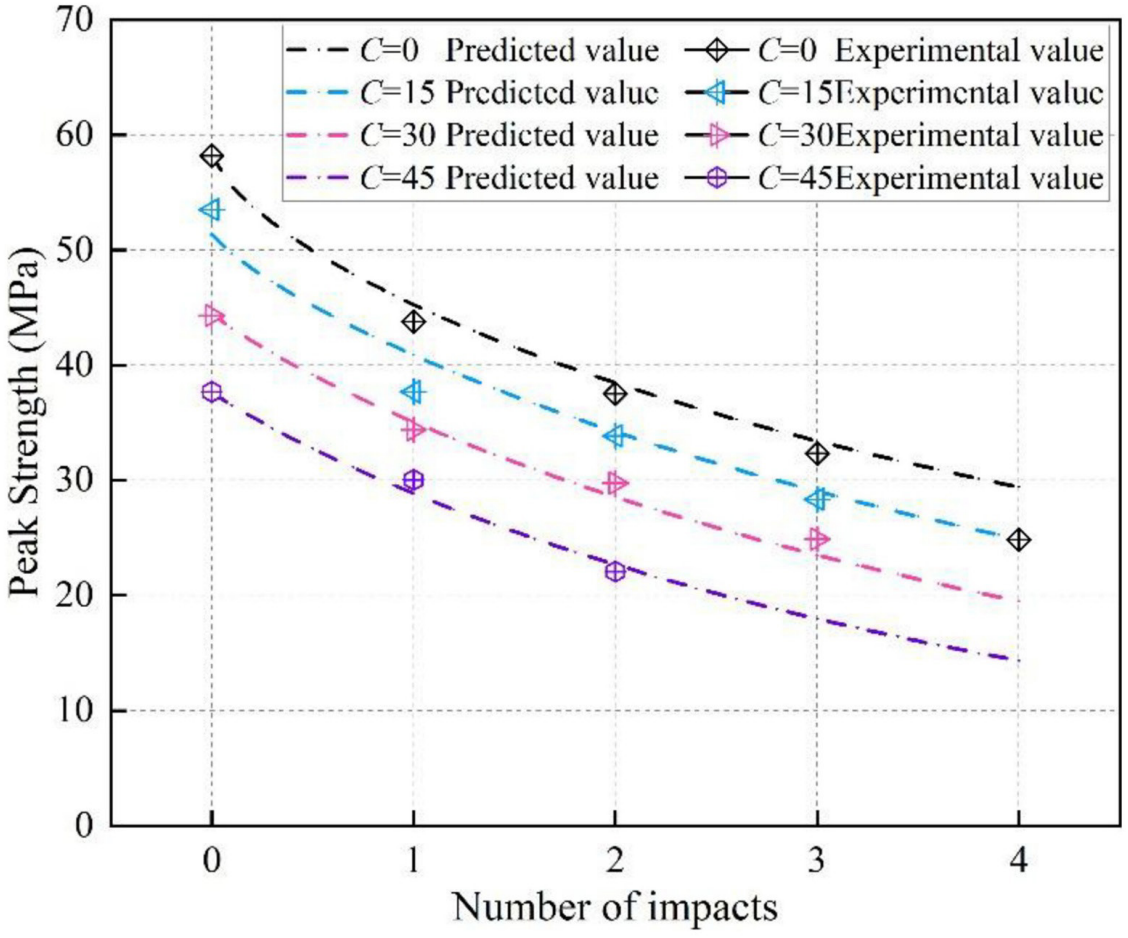

Figure 13. Comparison of results from the impact performance degradation model for CGC

4 Conclusions

To support the safe and efficient utilization of coal gangue (CG) as an aggregate in underground support structures, this study systematically investigated the dynamic response and damage evolution of coal gangue concrete (CGC) under single and cyclic impact loading. The principal findings are as follows:

Performance Evolution under Single Impact. The dynamic strength and elastic modulus of CGC exhibit a systematic decrease with higher CG replacement ratios, while peak strain increases. A fundamental shift in energy absorption mechanism occurs at high replacement levels—from matrix-dominated elastic storage to aggregate fragmentation and interface frictional dissipation. Although increased impact pressure enhances strength via strain-rate effects, it synergistically amplifies material fragmentation, particularly in high-CG-content mixes.

Damage Accumulation under Cyclic Impact. The fatigue life under cyclic impact deteriorates markedly with increased CG content. Damage evolution is governed by a "weak-phase-dominated" mechanism, where rapid micro-crack nucleation and coalescence at weak aggregate-matrix interfaces accelerate the degradation of stiffness and energy absorption capacity per cycle, leading to a pronounced reduction in total impact resistance.

Underlying Failure Mechanism. The impact-induced failure of CGC originates from the dual weakening effects: the low intrinsic strength of CG aggregates and the inferior bond of the interfacial transition zone. As the replacement ratio rises, the proliferation of these weak phases directs damage progression from localized interface cracking to a distributed network, culminating in a crushing-dominated failure mode governed by aggregate fragmentation and frictional slip. Consequently, the macro-scale energy absorption mechanism transitions from elastic to plastic dominance.

Predictive Model for Engineering Design. An impact performance degradation model was established that couples the CG replacement ratio with the number of impact cycles. This model quantitatively predicts the decay of dynamic mechanical properties, providing a theoretical basis for the performance-based design and residual life assessment of CGC support structures in dynamic disturbance environments, such as mine roadways.

Acknowledgements

The research work of the author was supported by the China Postdoctoral Science Foundation - CCTEG Joint Support Program (Grant No. 2025T027ZGMK), the China Postdoctoral Science Foundation (Grant No. 2025M771778), the Scientific Research Foundation for High-level Talents of Anhui University of Science and Technology (Grant No. YJ20240025), and the National Science and Technology Major Project on Clean and Efficient Coal Utilization and Energy Transition (Grant No. 2024ZD1700203).

Author's Contributions: Conceptualization, L Fan; Methodology, L Fan and Y Liu; Investigation, L Fan; Writing - original draft, L Fan, Y Liu and YQ Zhu; Funding acquisition, L Fan; Resources, L Fan; Supervision, L Fan.

Data Availability statement: Research data is available in the body of the article

Editor: Marcílio Alves

References

Cai, W., Dou, L.M., Si, G.Y., Hu, Y.W. (2021). Fault-induced coal burst mechanism under mining-induced static and dynamic stresses. Engineering 7(5):687–700. https://doi.org/10.1016/j.eng.2020.03.017

Chen, Q.G., Zuo, Y.J., Zheng, L.J. (2025). Deformation failure mechanism and stability-control technology of deep layered clastic-rock roadway under dynamic disturbance. Tunnelling and Underground Space Technology 156:106255. https://doi.org/10.1016/j.tust.2024.106255

Chin, S.C., Shaaban, I.G., Rizzuto, J.P., Khan, S.U., Mohamed, D., Roslan, N.I.M., Aziz, A.A. (2024). Predictive models for mechanical properties of hybrid fibres reinforced concrete containing bamboo and basalt fibres. Structures 61:106093. https://doi.org/10.1016/j.istruc.2024.106093

Deng, P.H., Zhang, Z.J., Tian, Y.K., Wu, L.L., Wang, M., Yang, Z., Tong, K.W., Hu, L. (2026). Fatigue damage mechanism and crack evolution law of central-boundary fractured sandstone under cyclic loading. Theoretical and Applied Fracture Mechanics 142:105416. https://doi.org/10.1016/j.tafmec.2025.105416

Du, P., Ren, Y.G., Liu, Z.F., He, J.J., Wang, L.T. (2025). From waste to resources: Coal gangue utilization—A comprehensive analysis. Process Safety and Environmental Protection 201:107558. https://doi.org/10.1016/j.psep.2025.107558

Fairhurst, C.E., Hudson, J.A. (1999). Draft ISRM suggested method for the complete stress–strain curve for intact rock in uniaxial compression. International Journal of Rock Mechanics and Mining Sciences 36:279–289.

Gong, F.Q. (2010). Experimental study on rock mechanical property and dynamic strength criteria under coupled static and dynamic loads, Ph.D. Thesis, Central South University (Changsha).

He, M.C., Wang, Q. (2023). Rock dynamics in deep mining. International Journal of Mining Science and Technology 33(9): 1065–1082. https://doi.org/10.1016/j.ijmst.2023.07.006

Hu, Z.M., Wang, J.F., Wang, F.Q., Shi, Z.Q., Hu, Z.Y. (2026). Mechanical behaviour of axially-loaded reinforced CGCC columns: Testing and numerical modelling. Engineering Structures 350:121924. https://doi.org/10.1016/j.engstruct.2025.121924

Jiao, Y.W., Qiao, J.Q., Jia, R.J., Wei, P.Y., Li, Y.Q., Ke, G.J. (2023). The influence of carbon imperfections on the physicochemical characteristics of coal gangue aggregates. Construction and Building Materials 409:133965. https://doi.org/10.1016/j.conbuildmat.2023.133965

Li, J.Y., Wang, J.M. (2019). Comprehensive utilization and environmental risks of coal gangue: A review. Journal of Cleaner Production 239:117946. https://doi.org/10.1016/j.jclepro.2019.117946

Liu, R.Z., Wang, S.M. (2025). Research progress on the comprehensive utilization of coal gangue. International Journal of Coal Preparation and Utilization. https://doi.org/10.1080/19392699.2025.2467736

MINISTRY OF GEOLOGY AND MINERAL RESOURCES OF THE PEOPLE'S REPUBLIC OF CHINA (1995). Testing procedures for physical and mechanical properties of rocks (DY-94). Geological Publishing House (Beijing).

Ni, T., Pei, X.J., Fan, M.M., Zhang, J.X. (2019). Experimental study on basic physical properties of SJP cement improved soil slurry. Bulletin of the Chinese Ceramic Society 38(8):2637–2641. https://doi.org/10.16552/j.cnki.issn1001-1625.2019.08.044

Qin, J., Zhang, H., Geng, Y., Moy, C.K.S., Wang, Y.Y. (2025). Creep behavior for concrete incorporating coal gangue coarse and fine aggregates. Journal of Building Engineering 111:113427. https://doi.org/10.1016/j.jobe.2025.113427

Song, Q., Yang, Y.X., Xu, S.P., Gao, S.J., Liu, J., Bao, J.W., Xue, S.B. (2025). Research progress on the performance and improvement of coal gangue concrete. Coal Science and Technology 53(2):407–425.

Wang, A.G., Hao, F.J., Liu, P., Mo, L.W., Liu, K.W., Li, Y., Cao, J.F., Sun, D.S. (2022). Separation of calcined coal gangue and its influence on the performance of cement-based materials. Journal of Building Engineering 51:104293. https://doi.org/10.1016/j.jobe.2022.104293

Wang, J.L., Chen, J.L., Liu, M. (2024). Theoretical model for CFRP-confined spontaneous combustion gangue coarse aggregate concrete-filled steel tube stub columns under axial compression. Construction and Building Materials 415:135113. https://doi.org/10.1016/j.conbuildmat.2024.135113

Wu, X.J., Zhao, H., Wang, R., Wang, Y.H., Cui, H.Z., Chen, M.T. (2025). Bending behaviour of raw coal gangue concrete-filled steel tubes. Structures 76:108989. https://doi.org/10.1016/j.istruc.2025.108989

Xiang, J.C., Qiu, J.P., Zhao, Y.Q., Zheng, P.K., Peng, H.N., Fei, X.C. (2024). Rheology, mechanical properties, and hydration of synergistically activated coal gasification slag with three typical solid wastes. Cement and Concrete Composites 147:105418. https://doi.org/10.1016/j.cemconcomp.2023.105418

Yang, Y.B., Chen, B.X., Zeng, W.Z., Li, Y.J., Chen, Q.H., Guo, W.Y., Wang, H.C., Chen, Y.Q. (2021). Utilization of completely recycled fine aggregate for preparation of lightweight concrete partition panels. International Journal of Concrete Structures and Materials 15(1):32. https://doi.org/10.1186/s40069-021-00470-z

Zhang, M.T., Fan, J.Y., Luan, M.Y., Chen, J., Jiang, D.Y., Wang, Y.F., Lu, D., Li, Z.Z., Nelias, D. (2026). Crack evolution in salt rock with a prefabricated flaw under uniaxial compression: Insights from coupled AE and DIC monitoring. Theoretical and Applied Fracture Mechanics 143(Part 1):105449. https://doi.org/10.1016/j.tafmec.2026.105449

Zhang, X.D., Dong, Y., Li, W.L., Zhang, Y., Su, L.J., Cai, G.J., Wu, Q. (2026). Study on the mechanical properties and fracture behavior of coal gangue aggregate concrete modified by physical-chemical composite. Theoretical and Applied Fracture Mechanics 143(Part 1):105452. https://doi.org/10.1016/j.tafmec.2026.105452

Zhang, Z.G., Xu, C., Cheng, G., Von Lau, E. (2025). Towards carbon neutrality: A comprehensive study on the utilization and resource recovery of coal-based solid wastes. International Journal of Coal Science and Technology 12(1):34. https://doi.org/10.1007/s40789-025-00775-4

Zhao, Z.Q., Cheng, X.F., Li, G.Q., Gu, X.Q., Wu, C., Gao, P.W. (2026). Fracture mechanical properties of ultra-high performance concrete under mode I/II mixed fracture: A study on the coupling effect of steel fiber content and crack-to-depth ratio. Theoretical and Applied Fracture Mechanics 143(Part 1):105451. https://doi.org/10.1016/j.tafmec.2026.105451

Zhou, X., Zhang, D.M., Nowamooz, H., Jiang, C.B., Ye, C. (2022). Investigation on damage and failure mechanisms of roadway surrounding rock triggered by dynamic-static combined loads. Rock Mechanics and Rock Engineering 55(9):5639–5657. https://doi.org/10.1007/s00603-022-02949-x